

UC Office of the President

Research Grants Program Office (RGPO) Funded Publications

Title

Site-specific antibody-drug conjugates with variable drug-to-antibody-ratios for AML therapy

Permalink

<https://escholarship.org/uc/item/9337j19k>

Authors

Dai, Zhefu

Zhang, Xiao-Nan

Cheng, Qinqin

et al.

Publication Date

2021-08-01

DOI

10.1016/j.jconrel.2021.06.041

Peer reviewed

Site-Specific Antibody-Drug Conjugates with Variable Drug-to-Antibody-Ratios for Acute Myeloid Leukemia Therapy

Zhefu Dai^{1#}, Xiao-Nan Zhang^{1#}, Qinqin Cheng¹, Fan Fei¹, Tianling Hou¹, Jiawei Li¹, Alireza Abdolvahabi², Junji Watanabe³, Hua Pei⁴, Goar Smbatyan⁵, Jianming Xie¹, Heinz-Josef Lenz⁵, Stan G. Louie⁴ and Yong Zhang^{1,6,7,8*}

¹Department of Pharmacology and Pharmaceutical Sciences, School of Pharmacy, University of Southern California, Los Angeles, CA 90089, USA

²Mass Spectrometry Core Facility, School of Pharmacy, University of Southern California, Los Angeles, CA 90089, USA

³Translational Research Laboratory, School of Pharmacy, University of Southern California, Los Angeles, CA 90089, USA

⁴Titus Family Department of Clinical Pharmacy, School of Pharmacy, University of Southern California, Los Angeles, CA 90089, USA

⁵Division of Medical Oncology, Norris Comprehensive Cancer Center, Keck School of Medicine, University of Southern California, Los Angeles, CA 90089, USA

⁶Department of Chemistry, Dornsife College of Letters, Arts and Sciences, University of Southern California, Los Angeles, CA 90089, USA

⁷Norris Comprehensive Cancer Center, University of Southern California, Los Angeles, CA 90089, USA

⁸Research Center for Liver Diseases, University of Southern California, Los Angeles, CA 90089, USA

[#]These authors contributed equally to this work

*Corresponding author. Email: yongz@usc.edu

Keywords: antibody-drug conjugate; acute myeloid leukemia; protein engineering; targeted therapy;

Abstract

Random conjugations of chemotherapeutics to monoclonal antibodies result in heterogeneous antibody-drug conjugates (ADCs) with suboptimal pharmacological properties. We recently developed a new technology for facile generation of homogeneous ADCs by harnessing human CD38 catalytic domain and its dinucleotide-derived covalent inhibitor, termed **ADP-ribose cyclase-enabled ADCs (ARC-ADCs)**. Herein we advance this technology by designing and synthesizing ARC-ADCs with customizable drug-to-antibody ratios (DARs). Through varying numbers and locations of CD38 fused to an antibody targeting human C-type lectin-like molecule-1 (hCLL-1), ARC-ADCs featuring DARs of 2 and 4 were rapidly generated via a single step with cytotoxic monomethyl auristatin F (MMAF) as payloads. In contrast to anti-hCLL-1 ARC-ADC carrying 2 drug molecules, anti-hCLL-1 ARC-ADC with a DAR of 4 shows highly potent activity in killing hCLL-1-positive acute myeloid leukemia (AML) cells both *in vitro* and *in vivo*. This work provides novel ADC candidates for combating AML and supports ARC-ADC as a general and versatile approach for producing site-specific ADCs with defined DARs.

Introduction

Antibody-drug conjugates (ADCs) can deliver small-molecule drugs covalently linked to the immunoglobulin scaffold to specific types of cells with surface-expressed target antigens.¹ Due to limitations on conjugation strategies,²⁻⁴ all currently approved ADCs are heterogeneous with varying locations and numbers of payloads. Each ADC used in clinic contains multiple populations with different drug-to-antibody ratios (DARs) that perform distinctively *in vivo*,^{5, 6} raising efficacy and safety concerns.

To develop homogeneous ADCs, different technologies have been established such as utilizing engineered amino acids and carbohydrates, incorporating unnatural amino acids, grafting peptides, and fusing protein domains for creating handles for conjugation.⁷⁻²² By exploiting enzymatic activity of human CD38, a member of ADP-ribosyl cyclase family, we recently developed a new approach for single-step generation of site-specific ADCs, named **ADP-ri**bosyl **c**yclase-enabled ADCs (ARC-ADCs).²³ Through a 2'-Cl-arabinose nicotinamide adenine dinucleotide (2'-Cl-araNAD⁺)-based covalent inhibitor of CD38, cytotoxic monomethyl auristatin F (MMAF) could be covalently attached to antibodies genetically fused with CD38 via its catalytic glutamate 226 (Glu226) residue (Figure 1A). The resulting ARC-ADC with a DAR of 2 shows excellent stability and efficacy in treating breast cancer in preclinical models.²³

Given the CD38-enabling nature for site-specific conjugation, we envisioned that ARC-ADCs may provide unique opportunities for facile production of homogeneous ADCs with customizable DARs. To test this notion, we designed and generated two forms of ARC-ADCs with DARs of 2 and 4, designated as DAR2-ARC-ADC and DAR4-ARC-ADC, respectively, which exhibit remarkable *in vitro* and *in vivo* efficacy against human acute myeloid leukemia (AML) cells through specifically targeting human C-type lectin-like molecule-1 (hCLL-1). AML is the most common type of acute leukemia in adults with 5-year survival rate below 30%.²⁴ CLL-1 is frequently overexpressed in blasts and leukemia stem cells (LSCs) of AML patients,²⁵ but absent on normal hematopoietic stem cells (HSCs) in bone marrow, representing a promising target for AML treatment.²⁶⁻³⁰ Our anti-hCLL-1 ARC-ADCs not only provide new therapeutic candidates for AML but also demonstrate ARC-ADC as a general approach for making homogeneous ADCs with tailored DARs.

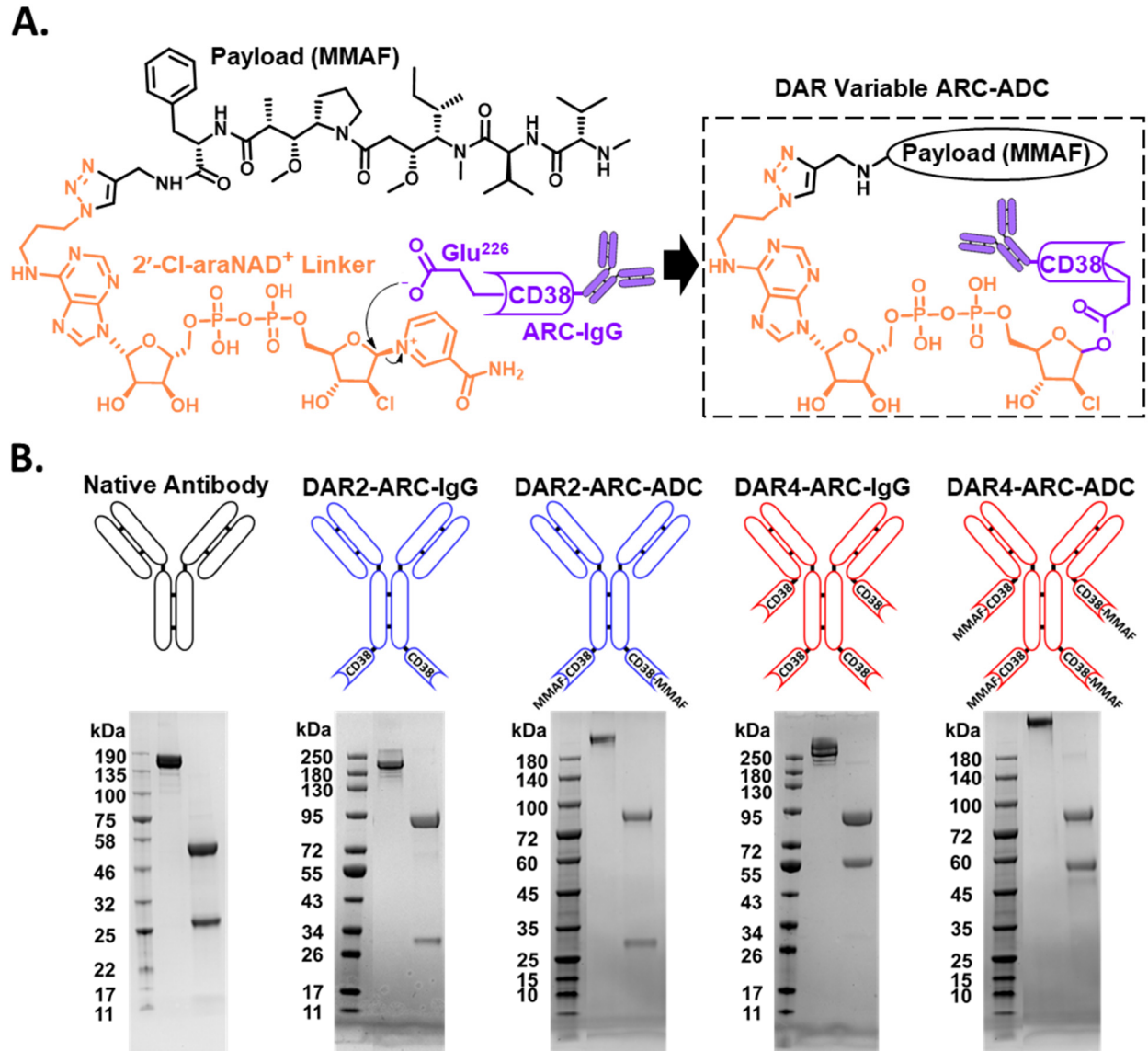


Figure 1. Homogeneous ARC-ADCs with variable DARs. (A) Schematic of 2'-Cl-araNAD⁺ linker-mediated site-specific antibody-drug conjugation. (B) Generation of anti-hCLL-1 IgG, anti-hCLL-1-CD38 C-fusions, and anti-hCLL-1 ARC-ADCs with DARs of 2 and 4. Lower panel: Coomassie-stained SDS-PAGE gels for purified anti-hCLL-1 IgG (native antibody), anti-hCLL-1-CD38 C-fusions (DAR2-ARC-IgG and DAR4-ARC-IgG), and anti-hCLL-1 ARC-ADCs.

Results

Since the DAR of an ARC-ADC is associated with the number of fused CD38 catalytic domain, fusing additional CD38 extracellular domains to the immunoglobulin scaffold may thus increase numbers of payloads, likely resulting in site-specific ADCs with enhanced potency. To this end, we genetically fused human CD38 enzymatic domain to C-termini of light chain (LC) and heavy chain (HC) of an anti-hCLL-1 monoclonal antibody 1075.7.³¹ The resulting HC-CD38 C-fusion construct was paired with LC or LC-CD38 C-fusion expression vector for transient transfection in mammalian cells for production of an anti-hCLL-1 IgG HC-CD38 C-fusion (denoted as DAR2-ARC-IgG) and an anti-hCLL-1 IgG HC-CD38 & LC-CD38 C-fusion (denoted as DAR4-ARC-IgG). Together with expressed native anti-hCLL-1 antibody, DAR2-ARC-IgG and DAR4-ARC-IgG were analyzed by Coomassie-stained SDS-PAGE gels (Figure 1B). The observed sizes of light and heavy chains for each construct are consistent with molecular designs. The yields are about 10 mg L⁻¹ and 7 mg L⁻¹ for DAR2-ARC-IgG and DAR4-ARC-IgG, respectively, lower than that of anti-hCLL-1 antibody (14 mg L⁻¹).

Next, CD38 enzymatic activity and hCLL-1 binding affinity were examined for DAR2-ARC-IgG and DAR4-ARC-IgG. Fluorescence-based activity assays indicated that both fusion IgGs possess significantly higher catalytic activities than that of recombinant human CD38 extracellular domain, possibly due to improved stability (Figure 2A). Reactions catalyzed by DAR4-ARC-IgG show approximate 50% rate increase relative to those by DAR2-ARC-IgG, owing to two extra CD38 domains. As a control, native anti-hCLL-1 antibody gives no enzymatic activity. Enzyme linked immunosorbent assay (ELISA) analysis revealed tight binding to recombinant hCLL-1 for both DAR2-ARC-IgG and DAR4-ARC-IgG, comparable to that of native anti-hCLL-1 antibody (Figure 2B). These results support successful generation of anti-hCLL-1-CD38 fusions with robust CD38 enzymatic activity and high affinity to hCLL-1 antigen, allowing rapid generation of anti-hCLL-1 ARC-ADCs with distinct DARs. Additionally, ELISA indicated that in contrast to the anti-hCLL-1 antibody, DAR2-ARC-IgG and DAR4-ARC-IgG exhibit slightly increased or comparable binding affinities to human CD16a and C1q (Figure S1), which are Fc receptor and complement protein, respectively, involved in activation of antibody-dependent cellular cytotoxicity and the classical complement pathway. This suggests that genetic fusions of the CD38

catalytic domain to the C-termini of antibody heavy and light chains may have no adverse impact on functions of the antibody Fc region.

Anti-hCLL-1 ARC-ADCs were then generated by incubating DAR2-ARC-IgG or DAR4-ARC-IgG with synthesized drug-linker conjugate (2'-Cl-araNAD⁺-MMAF) on ice for 1 hour, resulting in DAR2-ARC-ADC and DAR4-ARC-ADC (Figure 1B). As a tubulin inhibitor, MMAF is a potent cytotoxic payload. Mass spectrometry confirmed the generation of anti-hCLL-1 ARC-ADCs with DARs of 2 and 4 (Figure S2). *In vitro* cytotoxicity of the anti-hCLL-1 ARC-ADCs was then evaluated using human AML cell lines U937 (CLL-1⁺) and KG1a (CLL-1⁻¹) (Figure 2C-D). DAR4-ARC-ADC exhibits highly potent cytotoxicity ($EC_{50} = 25 \pm 8$ pM) against U937 cells and DAR2-ARC-ADC displays relatively lower potency with an EC_{50} of 0.9 ± 0.4 nM (Figure 2D). The drug-linker and ARC-IgGs have much weaker or little cytotoxicity for U937 cells. In comparison, none of these agents reveals significant toxicity for KG1a cells. These results demonstrate outstanding potency and specificity of anti-hCLL-1 ARC-ADCs and markedly enhanced efficacy for DAR4-ARC-ADC.

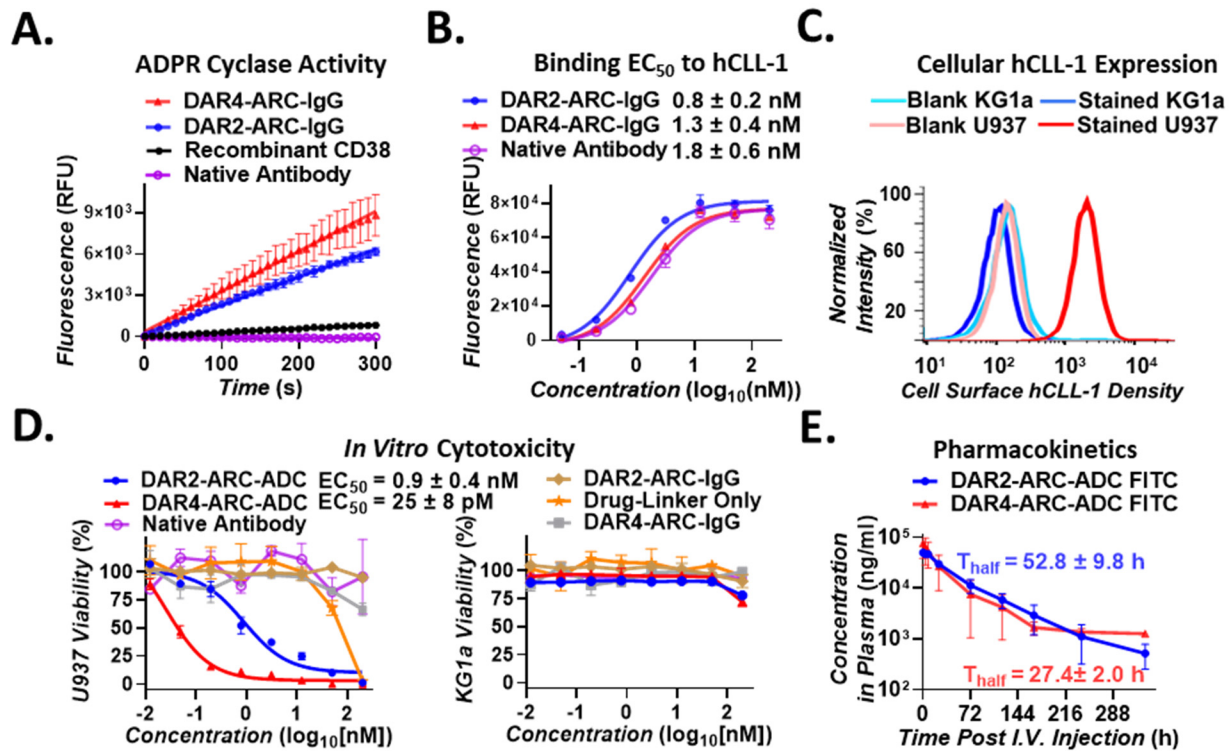


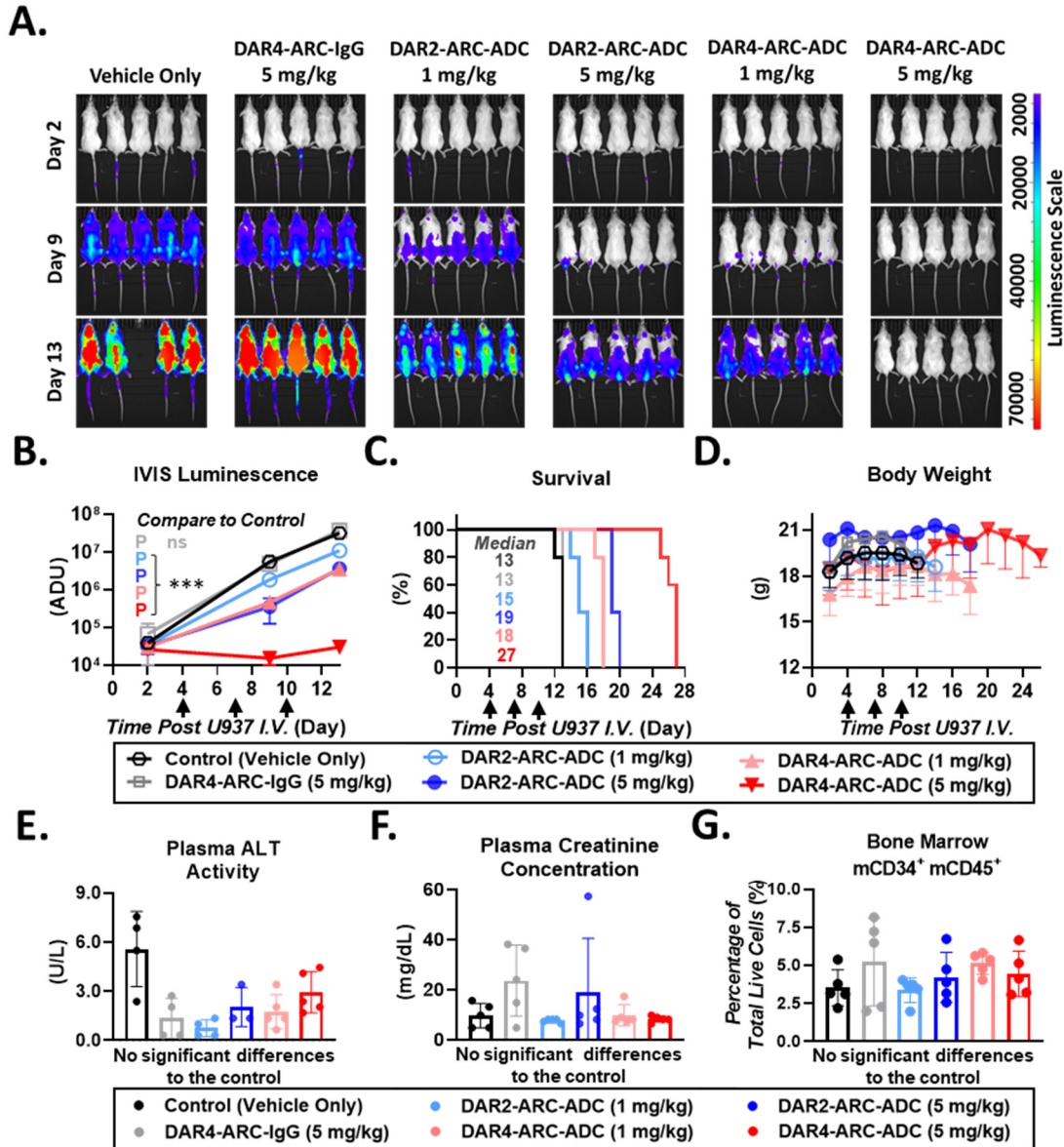
Figure 2. Characterization of anti-hCLL-1-CD38 C-fusions and anti-hCLL-1 ARC-ADCs. (A) Analysis of ADP-ribosyl cyclase activity. Purified CD38 (20 nM), anti-hCLL-1 antibody (10 nM), DAR2-ARC-IgG (10 nM), or DAR4-ARC-IgG (10 nM) was incubated with 100 μ M NGD⁺ in PBS to monitor ADPR cyclase activity based on the formation of fluorescent cyclic GDP-ribose at 410 nm. (B) ELISA analysis of binding to recombinant hCLL-1 extracellular domain. (C) Flow cytometric analysis of hCLL-1 expression on human U937 and KG1a cells. (D) *In vitro* cytotoxicity of DAR2-ARC-ADC and DAR4-ARC-ADC. U937 or KG1a cells were incubated for 72 hours at 37°C with 5% CO₂ with various concentrations of ARC-ADCs, drug-linker conjugate, native anti-hCLL-1 antibody, and ARC-IgGs. Cell viability was determined by MTT assays with data for cells incubated with culture medium or 5 μ M paclitaxel as 100% viable or 0% viable references, respectively. (E) Pharmacokinetics in mice for surrogate DAR2-ARC-ADC and DAR4-ARC-ADC with FITC as the payloads. Noncompartmental analysis was conducted based on the plasma concentrations of surrogate ARC-ADCs determined through a sandwich ELISA by utilizing an anti-FITC polyclonal antibody as capture antibody and an anti-human kappa light chain monoclonal antibody conjugated with HRP as detection antibody.

To examine stability, surrogate ARC-ADCs were generated using Alexa Fluor 488 or fluorescein isothiocyanate (FITC) as the payloads. In-gel fluorescence-based imaging revealed considerable stability for both surrogate DAR2-ARC-ADC and DAR4-ARC-ADC incubated in fresh mouse plasma (Figure S3). Pharmacokinetic studies were then performed in mice. Following single-dose intravenous (i.v.) injections of FITC-conjugated surrogate ARC-ADCs, sandwich ELISA assays were conducted for collected plasma samples by using anti-FITC and anti-human kappa light chains antibodies as capture and detection reagents. The measured plasma concentrations indicated a half-life of 52.8 ± 9.8 hours for DAR2-ARC-ADC FITC and 27.4 ± 2.0 hours for DAR4-ARC-ADC FITC (Figure 2E), suggesting reduced stability for ARC-ADC with increased payloads.

Next, *in vivo* therapeutic efficacy of DAR2-ARC-ADC and DAR4-ARC-ADC were evaluated using AML mouse xenograft models. Immunodeficient mice were intravenously injected with firefly luciferase-labeled U937 cells via tail vein. Beginning on day 4 post U937 cell implantation, mice were treated with ARC-ADCs at a dose of 1 or 5 mg/kg every 72 hours for a total of 3 times through i.v. injections. PBS vehicle and DAR4-ARC-IgG (5 mg/kg) were included as controls. From day 2 post i.v. implantation of luciferase-expressing U937 cells, whole-body luminescence imaging was taken for each group of mice and continued on a weekly basis. IVIS imaging and quantified luminescence indicated rapid proliferation of U937 cells for mice treated by PBS vehicle and DAR4-ARC-IgG. By contrast, administered ARC-ADCs show significant anti-leukemia activity in dose- and DAR-dependent manners (Figures 3A-B and S4). Notably, DAR4-ARC-ADC at the dose of 5 mg/kg displays highly potent inhibition against the proliferation of engrafted U937 cells. In comparison to PBS- and DAR4-ARC-IgG-treated groups with median survivals of 13 days, DAR4-ARC-ADC-treated group at 5 mg/kg shows more than 100% increase of median survival (27 days) (Figure 3C). Consistent with IVIS imaging analysis, the median survivals for mice treated by DAR2-ARC-ADC and DAR4-ARC-ADC are dependent on dose and DAR. Same as the *in vitro* cytotoxicity studies, *in vivo* results support excellent anti-leukemia activities for anti-hCLL-1 ARC-ADCs and significantly improved efficacy for DAR4-ARC-ADC.

Toxicities of the administered anti-hCLL-1 ARC-ADCs on mice were also assessed. During the efficacy study, treatments with ARC-ADCs cause no negative impact on mice body weights in comparison to control groups (Figure 3D). On day 13 after U937 implantation, plasma alanine

aminotransferase (ALT) activity and creatinine concentration and percentages of mouse CD34⁺ CD45⁺ cells in blood, bone marrow, and spleen samples were determined. No significant differences were observed among all groups (Figures 3E-G and S5). Taken together, these results show no apparent toxicity for anti-hCLL-1 ARC-ADCs.



In addition to IVIS imaging analysis, blood, bone marrow, and spleen were collected for all groups on day 13 post U937 implantation for flow cytometry. Consistent with the luminescence-based whole-body imaging, flow cytometric analysis indicate higher levels of engrafted U937 cells and lower percentages of mouse CD45⁺ (mCD45⁺) cells in bone marrow, spleen, and blood for mice treated by PBS and DAR4-ARC-IgG (Figure 4A-G). Less than 0.5% of hCLL-1⁺ cells were observed across 3 different types of tissues for mice treated by DAR2-ARC-ADC and DAR4-ARC-ADC at 5 mg/kg (Figure 4B-D), indicating their potent activities in suppressing U937 cells expansion. Relative to control groups, significantly higher percentages of mCD45⁺ were observed for mice treated by ARC-ADCs at both 1 and 5 mg/kg in bone marrow and at 5 mg/kg in spleen and blood (Figure 4F-G). Similar to the quantified luminescence intensities, the measured percentages of hCLL-1⁺ among different tissues for mice treated by ARC-ADCs inversely correlate with dose and DAR. In comparison to mice receiving DAR2-ARC-ADC at 1 mg/kg, DAR4-ARC-ADC-treated mice at 1 mg/kg revealed significantly lower percentages of hCLL-1⁺ cells in blood, bone marrow, and spleen (Figure 4B-D). Moreover, mice given with DAR4-ARC-ADC have higher levels of mCD45⁺ in bone marrow compared with DAR2-ARC-ADC-treated ones at both 1 and 5 mg/kg doses (Figure 4F). These results support remarkable efficacy for anti-hCLL-1 ARC-ADCs and considerably increased potency for DAR4-ARC-ADC.

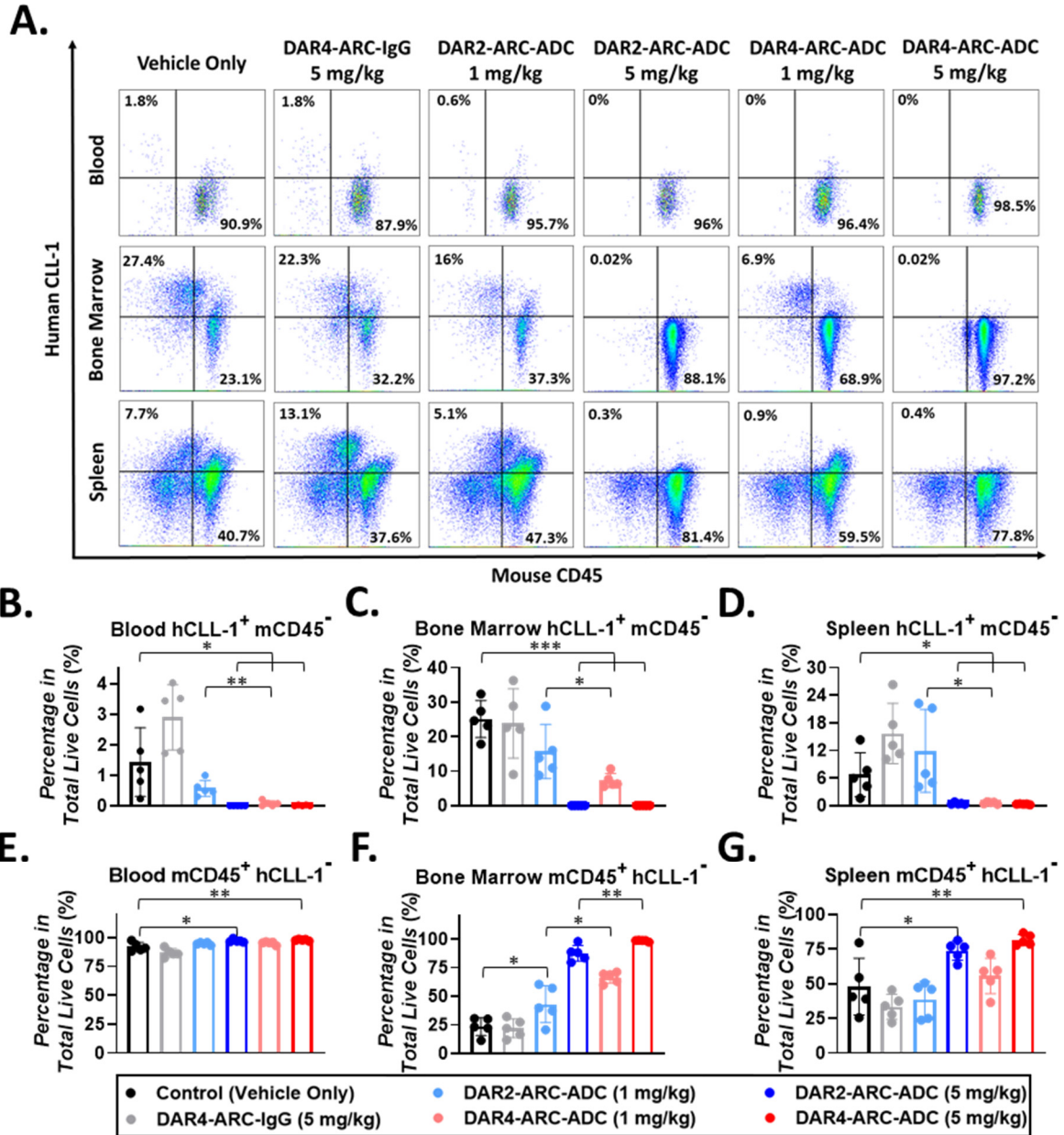


Figure 4. Flow cytometric analysis of tissue samples collected on day 13 post U937 implantation. (A) Representative flow cytometry data for hCLL-1 and mCD45 expression in blood, bone marrow, and spleen cells among different groups. Percentages were shown for hCLL-1⁺ mCD45⁻ and mCD45⁺ hCLL-1⁻ cells in total living cells. (B-D) Percentages of hCLL-1⁺ mCD45⁻ cells in total living cells in blood (B), bone marrow (C), and spleen (D) samples among different groups. (E-G) Percentages of mCD45⁺ hCLL-1⁻ cells in total living cell in blood (E), bone marrow (F), and spleen (G) among different groups.

Discussion

Anti-hCLL-1 ARC-ADCs were successfully generated with DARs of 2 and 4 by utilizing antibody-CD38 fusions coupled with an NAD⁺ analogue-derived drug linker. By specifically binding to hCLL-1 antigen, ARC-ADCs allow targeted delivery of tubulin inhibitor MMAF to human AML cells, resulting in potent *in vitro* and *in vivo* anti-leukemia activities. Despite reduced plasma half-life, DAR4-ARC-ADC exhibits notably enhanced potency in both cellular and animal AML models, revealing therapeutic benefits for developing homogeneous ADCs with increased DARs.

Genetic fusions of CD38 catalytic domains to an antibody enable facile production of site-specific ADCs through single-step enzymatic reactions. In addition to rapidly mediating drug conjugation at Glu226 of CD38, the 2'-Cl-araNAD⁺-based dinucleotide linker can stably carry payloads to target cells for rapid release upon internalization. The DARs of ARC-ADCs can possibly be adjusted by fusing additional CD38 domains to further increase efficacy. Meanwhile, attachments of CD38 to an immunoglobulin can potentially affect the overall stability of fusion proteins, binding affinity to target antigens, and tissue penetration.

DAR4-ARC-ADC was generated by fusing CD38 to C-termini of light and heavy chains of the anti-hCLL-1 antibody. Different formats of ARC-ADC with a DAR of 4 could be developed by placing CD38 at different positions. While having the same DAR, these ARC-ADC may possess distinguished physicochemical properties and biological activities, which requires further examination. By changing the fusion location or linkers used between the antibody and CD38 domain, stability and efficacy for ARC-ADCs could be further optimized. Importantly, ARC-ADCs with additionally increased DARs can potentially be synthesized and evaluated for pharmacological activities.

To understand how varied number of payloads affect cytotoxicity of ADCs, cellular uptake and drug release need to be quantitatively analyzed for ARC-ADCs with different DARs. The ARC-ADCs can also be extended to other types of payloads and antibodies specific for disease-associated antigens.

In summary, anti-hCLL-1 ARC-ADCs with DARs of 2 and 4 were generated through harnessing genetically fused CD38 catalytic activity. DAR4-ARC-ADC is highly potent in killing

CLL-1-positive AML cells both *in vitro* and *in vivo*, providing a new candidate for AML targeted therapy. This study demonstrates ARC-ADC as a general and versatile approach for developing homogeneous ADCs with defined DARs.

Materials and Methods

Molecular Cloning. Synthetic gBLOCK DNA fragment for recombinant human CLL-1 extracellular domain natural variant (Uniprot ID: Q5QGZ9, VAR_037669, amino acid I70-A265) with a 6*His tag fused at C terminus was purchased from Integrated DNA Technologies (IA, USA). The synthetic DNA fragment above was amplified by polymerase chain reaction (PCR) with primers incorporating DNA restriction enzyme cleavage sites for EcoRI and NheI at the 5' and 3' end, respectively. Primers used for amplification include CLL-1-Forward: 5'-CACGAATTCGATCGAGATGAAGAAGATGAACAAAC-3'; CLL-1-Reverse: 5'-CCAGCTAGCACTCACTAATGATGATGGTG-3'.

Synthetic gBLOCK DNA fragments for anti-human CLL-1 IgG light chain (LC) and heavy chain (HC) fragment of antigen binding (Fab) (clone 1075.7) were purchased from Integrated DNA Technologies (IA, USA). The anti-human CLL-1 IgG LC DNA fragment was amplified by PCR with primers incorporating DNA restriction enzyme cleavage sites for EcoRI and NheI at the 5' and 3' end, respectively. The full-length anti-human CLL-1 IgG HC was generated through overlap extension PCR using the anti-human CLL-1 Fab HC and human IgG1 Fc fragments using primers containing DNA restriction enzyme cleavage sites for EcoRI and NheI at the 5' and 3' end, respectively. Primers mentioned above include Anti-CLL-1 IgG LC F: 5'-CACGAATTCGGAGAACGTGCTCACCCAATCCCC-3'; Anti-CLL-1 IgG LC R: 5'-CCAGCTAGCACTTATCAAACTCTCCCCTGTTGAAGCTCTTTGTG-3'; Anti-CLL-1 IgG HC F1: 5'-CACGAATTCGGACATCCAGCTGCAGGAGAGCG-3'; Anti-CLL-1 IgG HC R1: 5'-CGCAAGATTTGGGTTCCACTTTCTTGTCCACCTTGGTGTTGCTG-3'; Anti-CLL-1 IgG HC F2: 5'-GGTGGACAAGAAAGTGGAACCCAAATCTTGCGACAAAACCTCACACATG-3'; Anti-CLL-1 IgG HC R2: 5'-CCAGCTAGCACTTATCATTTACCCGGAGACAGGGAGAGGC-3'.

Acquired PCR products were then analyzed by DNA gel electrophoresis with the bands at target sizes excised and purified by DNA gel extraction kits (Zymo Research, CA, USA) to yield

the target DNA fragment inserts. Purified DNA fragment inserts were first treated with DNA restriction enzyme EcoRI and NheI (New England Biolabs, MA, USA) per the manufacturer's instructions and then cleaned by DNA cleaning & concentrating kits (Zymo Research, CA, USA). The treated and cleaned DNA fragments were then spliced in-frame to pFUSE expression vector backbone by T4 DNA ligase (New England Biolabs, MA, USA). Ligation products were utilized to transform DH10B *Escherichia coli* (*E. coli*) electro-competent cells, followed with positive selection for Zeocin-resistant colonies and DNA sequencing of the extracted plasmids.

The sequence-confirmed pFUSE expression vectors for anti-human CLL-1 IgG LC and anti-human CLL-1 IgG HC were utilized as DNA templates for constructing anti-CLL-1 IgG LC CD38 C-fusion and anti-CLL-1 IgG HC CD38 C-fusion pFUSE expression vectors, respectively. Synthetic gBLOCK DNA fragment of the extracellular domain of human CD38 (Uniprot ID: P28907, R45-I300) with four mutated asparagine residues (N100D, N164A, N129D, and N209D) and a flexible GGGGS linker at N-terminus was purchased from Integrated DNA Technologies (IA, USA). Overlap extension PCR reactions were performed to generate LC-CD38 C-fusion and HC-CD38 C-fusion fragments. Primers utilized for cloning include Anti-CLL-1 LC CD38 F1: 5'-GTCACGAATTCGGAGAACGTGCTC-3'; Anti-CLL-1 LC CD38 R1: 5'-CGCCACCCCCACACTCTCCCCTGTTGAAGCTCTTTG-3'; Anti-CLL-1 LC CD38 F2: 5'-GGAGAGTGTGGGGGTGGCGGAAGC-3'; Anti-CLL-1 LC CD38 R2: 5'-CTGGCCAGCTAGCACTTATCAGATCTC-3'; Anti-CLL-1 HC CD38 F1: 5'-CACGAATTCGGACATCCAGCTGCAGGAGAGCG-3'; Anti-CLL-1 HC CD38 R1: 5'-CGCAAGATTTGGGTTCCACTTTCTTGTCCACCTTGGTGTGCTG-3'; Anti-CLL-1 HC CD38 F2: 5'-GGTGGACAAGAAAGTGAACCCAAATCTTGCGACAAAACCTCACACATG-3'; Anti-CLL-1 HC CD38 R2: 5'-CTGGCCAGCTAGCACTTATCAGATCTC-3'.

Acquired PCR products were then analyzed by DNA gel electrophoresis with the bands at target sizes excised and purified by DNA gel extraction kits (Zymo Research, CA, USA) to yield the target DNA fragment inserts. Purified DNA fragment inserts were first treated with DNA restriction enzyme EcoRI and NheI (New England Biolabs, MA, USA) per the manufacturer's instructions and then cleaned by DNA cleaning & concentrating kits (Zymo Research, CA, USA). The treated and cleaned DNA fragments were then spliced in-frame to pFUSE expression vector backbone by T4 DNA ligase (New England Biolabs, MA, USA). Ligation products were utilized

to transform DH10B *E. coli* electro-competent cells, followed with positive selection for Zeocin-resistant colonies and DNA sequencing of the extracted plasmids.

Protein Expression and Purification. Recombinant human CD38 extracellular domain, human CLL-1 extracellular domain, anti-hCLL-1 IgG, anti-hCLL-1 IgG HC-CD38 C-fusion (DAR2-ARC-IgG), and anti-hCLL-1 IgG HC-CD38 & LC-CD38 C-fusion (DAR4-ARC-IgG) were all expressed in Expi293F cells (Thermo Fisher Scientific, MA, USA). Sequence-confirmed pFUSE expression vector for human CD38 (240 µg), CLL-1 (240 µg), or antibody light chain (120 µg) combined with heavy chain (120 µg) in 12 mL of Opti-MEM medium (Thermo Fisher Scientific, MA, USA) was added with 960 µL of transfection-grade linear polyethylenimine hydrochloride at 1 mg mL⁻¹ (Polysciences, PA, USA) for transfecting 240 mL of Expi293F cells cultured at a density of 2.5 million cells per mL per manufacturers' instructions. Cells were then incubated with shaking (125 rpm) in a 37°C incubator with 5% CO₂. On day 5 post transfection, media containing target proteins were collected. Cells were removed by a 2-step serial centrifugation with centrifugal force at 100 ×g for 10 minutes first, followed by 4,000 ×g for 30 minutes.

The recombinant human CD38 and CLL-1 extracellular domains were purified by the same protocol as previously reported.²³ In brief, media with target proteins were first dialyzed against storage buffer for overnight (25 mM HEPES, 250 mM NaCl, pH 7.5) before applying to the Ni-NTA resin-based affinity chromatography. Dialyzed media were gradually loaded onto a gravity-flow column with 1 mL of Ni-NTA resin and let passing through the resin twice, followed by washing with 15 column volumes of wash buffer (20 mM Tris-HCl, 200 mM NaCl, 30 mM imidazole, pH 8). Recombinant proteins were eluted in 15 column volumes of elution buffer (20 mM Tris-HCl, 200 mM NaCl, 400 mM imidazole, pH 8) and dialyzed into PBS buffer (pH 7.4) for overnight at 4°C and then in the same freshly prepared buffer for another 8 hours under the same condition. Finally, recombinant proteins were concentrated with 10 kDa-cutoff concentrators (MilliporeSigma, MA, USA). The purified proteins were examined by Coomassie blue stained SDS-PAGE gels. Protein concentrations were determined by UV absorbance at 280 nm with a NanoDrop 2000C spectrophotometer (Thermo Fisher Scientific, MA, USA) corrected by calculated molar extinction coefficients.

All antibodies were purified by protein G affinity chromatography resins (GenScript, NJ, USA) per the manufacturer's protocol. Antibodies were eluted by 15 column volumes of 100 mM glycine

(pH 2.7) and then dialyzed against PBS buffer (pH 7.4). After being concentrated by 30 kDa-cut-off concentrators (MilliporeSigma, MA, USA), the purified antibodies were examined by Coomassie blue stained SDS-PAGE gels. Protein concentrations were determined based on UV absorbance at 280 nm (corrected by calculated molar extinction coefficients) by a NanoDrop 2000C spectrophotometer.

Preparation of Drug-Linker Conjugate (2'-Cl-araNAD⁺-MMAF). 2'-Cl-araNAD⁺-MMAF was synthesized as reported previously.²³ To a stirred solution of 2'-Cl-NAD⁺-N₃ (7.7 mg, 0.01 mmol), CuSO₄·5H₂O (10.0 mg, 0.04 mmol, 4 eq) in H₂O (0.5 mL) were added a solution of alkynyl-MMAF (9.2 mg, 0.012 mmol, 1.2 eq) in DMSO (0.2 mL), THPTA (86.9 mg, 0.2 mmol, 20 eq) and sodium-L-ascorbate (63.4 mg, 0.32 mmol, 32 eq) at room temperature. Then the reaction mixture was stirred at the same temperature until the reaction completed (monitored by HPLC). The product was purified via preparative HPLC (C18-A column, 150×10.0 mm, 5 μm) (mobile phase A: 0.1% formic acid (aq), mobile B: 0.1% formic acid in acetonitrile; flow rate = 2.0 mL/min; 0-2 min: 0-4% B, 2-4 min: 4-10% B, 4-6 min: 10-20% B, 6-12 min: 20-50% B, 12-17 min: 50-100% B, 17-20 min: 100-0% B) with detection of UV absorbance at 260 nm. Fractions containing the desired product were concentrated and lyophilized to yield the compound 2'-Cl-NAD⁺-MMAF (8.4 mg, 55%) as a colorless solid. HRMS (ESI) for C₆₆H₉₇ClN₁₆O₂₀P₂Na₂²⁺ (M+2Na-2H)²⁺: Calcd.: 789.3085 Da; Obs: 789.3092 Da.

Preparation of ADCs and ADC Surrogates. DAR2-ARC-IgG and DAR4-ARC-IgG at above 10 μM stock concentrations were combined with the drug-linker conjugate (2'-Cl-araNAD⁺-MMAF) in Tris buffer (50 mM Tris, pH 8.5) at a final molar concentration ratio of 1:200 (antibody : drug-linker conjugate) on ice for 1 hour. Then, buffer exchange was performed using PBS and filters with 30 kDa cut-off (MilliporeSigma, MA, USA) to remove free drug-linker conjugate.

To generate ADC surrogates with Alexa Fluor 488 or FITC as the payload, the linker 2'-Cl-araNAD⁺-N₃ was first conjugated to DAR2-ARC-IgG or DAR4-ARC-IgG with the same method described above. Then, acquired fusion antibody-linkers were incubated with Alexa Fluor 488 DBCO (Click Chemistry Tools, AZ, USA) or DBCO-PEG3-FITC (CONJU-PROBE, CA, USA) in PBS buffer (pH 7.4) at a molar ratio of 1:50 (antibody-linker : fluorescent dye) for 30 minutes on ice. Finally, buffer exchange was performed using PBS (pH 7.4) and filters with 30 kDa cut-

off to remove free surrogate payloads. The concentrations of generated ADCs and ADCs surrogates were determined by Bradford assay kits (Thermo Fisher Scientific, MA, USA).

***In Vitro* Plasma Stability of Alexa Fluor 488-Conjugated Surrogate ADCs.** Exendin-4 (GenScript, NJ, USA) at a concentration of 3 mg mL⁻¹ was labeled with 1 mM *N*-hydroxysuccinimide (NHS)–fluorescein (Thermo Fisher Scientific, MA, USA) on ice for 2 hours in PBS buffer (pH 7.4). Then, the reaction mixture was passed through Zeba spin desalting columns (Thermo Fisher Scientific, MA) with molecular weight cut-off at 7 kDa for removing free NHS-fluorescein.

Acquired fluorescein-labeled exendin-4 (0.75 mg mL⁻¹) and Alexa Fluor 488-conjugated surrogate DAR2-ARC-ADC (3 μM) and DAR4-ARC-ADC (3 μM) were incubated in fresh CD-1 mouse plasma containing 100 μg mL⁻¹ of penicillin-streptomycin (Thermo Fisher Scientific, MA) in a 37°C incubator with 5% CO₂ for 14 days. During the incubation, 1 μL of mixture was periodically extracted and frozen at -20°C until the final SDS-PAGE gel analysis. Prior to Coomassie staining, SDS-PAGE gels were imaged by a ChemiDoc Touch Imager (Bio-Rad, CA, USA) for the presence of intact conjugated surrogate ADCs or fluorescein-labeled exendin-4 under the fluorescence mode. The intensity of fluorescent bands on SDS-PAGE gels were quantified by Image Lab (Bio-Rad, CA, USA).

Matrix-Assisted Laser Desorption Ionization Time-of-Flight Mass Spectrometry (MALDI-TOF MS) for IgG Modification Analysis. DAR2-ARC-IgG, DAR2-ARC-ADC, DAR4-ARC-IgG, and DAR4-ARC-ADC (~2 mg/mL) were deglycosylated with PNGase F (450 U mL⁻¹) in the presence of 10 mM DTT, and mixed with 2,6 dihydroxyacetophenone (DHAP) solution (20 mg mL⁻¹ in 50% acetonitrile:0.1% formic acid) at a ratio of 1:5 (by volume). Half microliter of each solution was spotted on a 384-Big Anchor MALDI target and let dry at room temperature. Crystallized samples were then analyzed using Bruker Rapiflex MALDI-TOF MS equipped with a Smartbeam 3D, 10 kHz, 355 nm Nd:YAG laser. The laser parameters were optimized as follows: scan range = 26 μm; number of shots per sample = 1000; laser frequency = 5000 Hz. The mass spectrometer was calibrated for high-mass range using protein A and trypsinogen standards under a linear mode. Data were analyzed using FlexAnalysis software and plotted using GraphPad Prism (CA, USA).

ADP-Ribosyl Cyclase Activities. Acquired recombinant human CD38 extracellular domain, DAR2-ARC-IgG, DAR4-ARC-IgG, and the anti-hCLL-1 antibody were all diluted to the final concentration of 20 nM for CD38 or 10 nM for antibody or ARC-IgGs in 100 μ L of PBS buffer (pH 7.4) with 100 μ M of nicotinamide guanine dinucleotide (NGD⁺). The rate of cyclic guanine dinucleotide phosphate-ribose (cGDPR) generation was monitored by a Synergy H1 plate reader (BioTek, VT, USA) for its signature fluorescence (excitation at 300 nm; emission at 410 nm) for 5 minutes.

Binding to Recombinant Human CLL-1. Purified recombinant human CLL-1 extracellular domain was coated overnight on 96-well ELISA plates at room temperature (Greiner Bio-One, NC) in 80 μ L of PBS buffer (pH 7.4) at a final concentration of 50 μ g mL⁻¹. Then, coated wells were blocked with PBS (pH 7.4) containing 3% bovine serum albumin (BSA) (MilliporeSigma, MA, USA) for 2 hours at room temperature followed by a three-time-wash with 200 μ L of 0.05% Tween-20-containing PBS (pH 7.4) buffer (PBST). Next, anti-CLL-1 antibody, DAR2-ARC-IgG, and DAR-4-ARC-IgG in PBS buffer (pH 7.4) were added into wells at a gradient of concentrations and let incubated at room temperature for 1 hour. After a three-time-wash by 0.05% PBST buffer (pH 7.4), 80 μ L of 1000-fold diluted anti-human kappa light chain antibody with conjugated horse reddish peroxidase (HRP) (Thermo Fisher Scientific, MA, USA) in PBS buffer (pH 7.4) were added and let incubated at room temperature for 1 hour followed by a three-time-wash by 0.05% PBST buffer (pH 7.4). Finally, 80 μ L of QuantaBlu fluorogenic substrate (Thermo Fisher Scientific, MA, USA) was added into wells. Fluorescence intensities (excitation at 325 nm; emission at 420 nm) were recorded by a Synergy H1 Plate Reader after a 5-minute incubation at room temperature. The results were analyzed by GraphPad Prism software for calculating the EC₅₀ for different antibody constructs binding to the recombinant human CLL-1 extracellular domain.

Binding to Human CD16a and C1q. Anti-hCLL-1 antibody, DAR2-ARC-IgG, and DAR4-ARC-IgG in PBS (pH 7.4) at various concentrations were incubated in the 96-well ELISA plates at room temperature for overnight. Wells were then blocked with PBS (pH 7.4) with 3% BSA for 2 hours at room temperature, followed by a three-time-wash with 200 μ L of 0.05% PBST buffer (pH 7.4). Human CD16a-Fc chimera with a 6 \times His-tag (150 nM in PBS (pH 7.4), R&D Systems, MN) or human C1q protein (50 nM in PBS (pH 7.4), Quidel Corporation, CA) was added into the wells

and incubated at room temperature for 2 hours. Following a three-time-wash with 200 μL of 0.05% PBST buffer (pH 7.4), an anti-6 \times His-tag antibody-HRP conjugate (50-fold dilution, Santa Cruz Biotechnology, TX) for bound CD16a or an anti-human C1q antibody-HRP conjugate (200-fold dilution, Invitrogen, MA) for bound C1q was added and incubated at room temperature for 2 hours. After a three-time-wash with 200 μL of 0.05% PBST buffer (pH 7.4), QuantaBlu fluorogenic substrate was added into wells. Fluorescence intensities (excitation at 325 nm; emission at 420 nm) were recorded by a Synergy H1 Plate Reader after a 5-minute incubation at room temperature. The results were analyzed by GraphPad Prism software for calculating the EC_{50} for binding of recombinant human CD16a and human C1q to different antibody constructs.

***In Vitro* Cytotoxicity of ADCs.** U937 or KG1a cells in RPMI1640 medium (Corning, NY, USA) supplemented with 10% FBS (Thermo Fisher Scientific, MA, USA) and 100 $\mu\text{g mL}^{-1}$ penicillin-streptomycin (Thermo Fisher Scientific, MA, USA) at passage 3 were placed into 96-well plates (5,000 cells per well) (Corning, NY, USA) in a total volume of 100 μL per well. For the positive control wells, paclitaxel (MilliporeSigma, MA) was added to the final concentration of 5 μM . For the treatment group wells, DAR2-ARC-ADC and DAR4-ARC-ADC were added in a gradient of concentrations. For other control groups wells, anti-CLL-1 antibody, DAR2-ARC-IgG, DAR4-ARC-IgG, or 2'-Cl-araNAD⁺-MMAF were added in a gradient of concentrations. After a 72-hour incubation in a 37°C incubator with 5% CO₂, 10 μL MTT reagent (Thermo Fisher Scientific, MA) was added into each well and let incubated for 2 hours in a 37°C incubator with 5% CO₂. Then, 100 μL of lysis buffer (20% SDS and 50% dimethylformamide dissolved in water, pH 4.7) was added and let incubated for 1 hour at 37°C. Finally, absorbance at 580 nm was measured with a Synergy H1 plate reader (BioTek, VT, USA). The average readings from the positive control wells were designated as 0% viability, while the average readings from wells containing only cells with culture medium and antibiotics were designated as 100% viability. The data were fitted by the sigmoidal function in GraphPad Prism to calculate EC_{50} values.

Generation of Luciferase-Expressing U937 Cell Line. HEK293T cells were maintained to achieve 70-95% confluence in DMEM medium (Corning, NY, USA) with 10% FBS. The pCDH-FFluc-GFP plasmid was used to transfect HEK293T cells together with packaging plasmids (pRRE, pVSVG, and pREV) with the calcium-phosphate transfection method. The lentivirus was collected and concentrated using filters with the molecular weight cut-off at 100 kDa (Thermo

Fisher Scientific, MA, USA). U937 cells (approximately 5×10^5 cells) were then loaded on a 24-well plate together with the concentrated lentivirus for centrifugation at 2,200 rpm for 90 minutes. The cells were washed twice into fresh RPMI1640 medium on the next day. After the transduced U937 cells cultured in RPMI1640 medium supplemented with 10% FBS reached a total number of 3 million, cells were harvested by centrifugation at $100 \times g$ for 5 minutes and resuspended in DPBS (Corning, NY, USA) containing 10% FBS for sorting based on intracellular green fluorescence protein (GFP) intensity on a BD FACSAria Fusion Cell Sorter (CA, USA). Data were analyzed by FACSDiva (CA, USA) and top 5% of U937 cells with the strongest GFP fluorescence intensity were selected for the *in vivo* study.

Pharmacokinetics of Surrogate ADCs with FITC as the Payload. Female CD-1 mice (Jackson Laboratory, ME, USA) at age of 6 weeks were randomly grouped into 5 mice per group. Surrogate ADCs with FITC as the payload at a dose of 5 mg kg^{-1} were administered by tail vein intravenous (I.V.) injection. Blood samples were collected at various time points throughout the 14-day-long study by tail venipuncture and processed for plasma samples by Multivette 600 μL lithium heparin gel collection tubes (Sarstedt Inc., Germany) per manufacturer's protocol. To detect the presence of intact surrogate ADCs by ELISA, anti-FITC polyclonal antibody (Thermo Fisher Scientific, MA, USA) at $8 \mu\text{g mL}^{-1}$ in PBS buffer (pH 7.4) was first coated on high-binding ELISA plates (Greiner Bio-One, Austria) at $80 \mu\text{L}$ per well for overnight at room temperature. After a 3-time-wash by 0.05% PBST buffer (pH 7.4), 100-fold diluted plasma samples in PBS buffer (pH 7.4) were applied into wells and let incubated at room temperature for 2 hours followed by a 3-time-wash by 0.05% PBST buffer (pH 7.4). Next, $80 \mu\text{L}$ of 1000-fold diluted goat anti-human kappa light chain antibody with HRP (Thermo Fisher Scientific, MA, USA) in PBS buffer (pH 7.4) was added and let incubated for 1 hour at room temperature followed by a 3-time-wash by 0.05% PBST buffer (pH 7.4). Finally, $80 \mu\text{L}$ of QuantaBlu fluorogenic substrate (Thermo Fisher Scientific, MA) was added. Fluorescence intensity of each well (excitation at 325 nm; emission at 420 nm) was recorded by a Synergy H1 plate reader (BioTek, VT, USA). Standards for different concentrations of surrogate ADCs were prepared by diluting surrogate ADCs into fresh CD-1 mice plasma, and fluorescence signals corresponding to each standard concentration were acquired by the same method mentioned above. Concentrations of surrogate ADCs in plasma samples were calculated based on a standard curve of fluorescence-concentration extrapolated from the standards.

Noncompartmental analysis in MatLab SimBiology (MathWorks, MA, USA) was employed to analyze pharmacokinetic parameters of surrogate ADCs.

In Vivo Efficacy Study. Female NOD.Cg-*Prkdc^{scid} Il2rg^{tm1Wjl}/SzJ* (NSG) mice at age of 6 weeks were purchased from the Jackson Laboratory (ME, USA). Each mouse was inoculated with 1 million luciferase-expressing U937 cells in 200 μ L DPBS by tail vein I.V. injection. On day 2 post U937 cells implantation, mice were randomized into 5 per group and given 150 mg kg⁻¹ of D-luciferin (Syd Labs, MA, USA), followed by imaging using an IVIS Lumina III Imaging System (PerkinElmer, MA, USA) for luminescence generated by luciferase-expressing U937 cells. On days 4, 7, and 10 post U937 cells inoculation, different groups of mice were given one of the following treatment options: (1) 200 μ L of DPBS (vehicle only); (2) DAR4-ARC-IgG at 5 mg kg⁻¹; (3) DAR2-ARC-ADC at 1 mg kg⁻¹; (4) DAR2-ARC-ADC at 5 mg kg⁻¹; (5) DAR4-ARC-ADC at 1 mg kg⁻¹; (6) DAR4-ARC-ADC at 5 mg kg⁻¹. In order to conduct both the interim efficacy analysis (when conditions of control group mice reach the endpoint per IACUC protocol) based on tissue sample analysis by flow cytometry as well as study for survival difference between groups, 2 groups of mice were given treatment option (3), (4), (5) or (6) with one group for interim efficacy analysis while the other group for survival analysis. Since the completion of first IVIS imaging, all live mice were continued to be imaged by IVIS weekly.

When mice in the control group (treatment option (1)) reached the humane endpoint, they were euthanized together with other groups of mice given the treatment option (2)-(6). Blood, spleen, and bone marrow samples were collected from each group, and samples were prepared into single cell suspension with red blood cells lysed by red blood cell lysis buffer (Biolegend, CA, USA) in DPBS containing 2% FBS. Prepared tissue samples were stained with anti-mouse CD34 PE antibody (119308, Biolegend, CA, USA), anti-mouse CD45 Pacific Blue antibody (MCD4528, Thermo Fisher Scientific, MA), anti-human CLL-1 APC antibody (353606, Biolegend, CA, USA), and propidium iodide (Thermo Fisher Scientific, MA). All samples were acquired by a BD LSRFortessa X-20 Cell Analyzer (CA, USA) and analyzed by FACSDiva and FlowJo software. Data for blood samples were first gated based on morphology (FSC-A/SSC-A) for peripheral blood myeloid cell population and then all live cells (propidium iodide-staining negative) populations were analyzed on fluorescence intensities of different antibodies used for staining. Data for spleen and bone marrow samples were first gated based on morphology (FSC-A/SSC-A) to remove non-

cell debris, and then all live cells (propidium iodide-staining negative) populations were analyzed on fluorescence intensities of different antibodies used for staining. Gating strategies for all samples were shown in Figures S6-S8.

For toxicology study, part of the blood samples collected during the interim efficacy analysis study were processed for plasma samples by Multivette 600 μL lithium heparin gel collection tubes (Sarstedt Inc., Germany) per manufacturer's protocol and frozen at -80°C . To measure the concentration of creatine in plasma, thawed plasma samples were first deproteinized by mixing with equal volume of 1.2 M trichloroacetic acid (Oakwood Chemicals, SC, USA) and the supernatants after centrifugation at $10,000 \times g$ for 5 minutes were then mixed with twice the volume of working solution, containing 38 mM picric acid premixed with equal volume of 1.2 M NaOH. After incubation at room temperature for 20 minutes, absorbance at 510 nm were recorded by a Synergy H1 plate reader (BioTek, VT, USA). Creatine powder (MilliporeSigma, MA, USA) was prepared into a series of concentrations of standards and utilized in the assay mentioned above for extrapolating a standard curve.

To measure alanine aminotransferase (ALT) activity in plasma, 5 μL of thawed plasma samples were first mixed with 25 μL of substrate solution (0.2 M alanine and 2 mM 2-oxoglutarate in 0.1 M disodium phosphate, pH 7.4) for 1 hour at 37°C . Then, the mixture was added with 25 μL of 1 mM 2,4-dinitrophenylhydrazine in 1 M HCl for 20 minutes at room temperature, followed by addition of 250 μL of 0.5 M NaOH. Absorbance at 510 nm was then measured by a Synergy H1 plate reader (BioTek, VT, USA). Pyruvate powder (MilliporeSigma, MA, USA) was prepared into a series of concentrations of standards and used to replace plasma samples in the above protocol for extrapolating a standard curve.

Statistical Analysis. Two-tailed unpaired t tests were performed for comparison between two groups. Tumor growth curves of the control and treatment groups were analyzed using two-tailed unpaired t tests. $P < 0.05$ was defined as statistically significant. Data are shown as mean \pm SD. Kaplan-Meier method was adopted to compare survival time between two groups of mice. All statistical analyses were performed using GraphPad Prism.

Acknowledgements

This work was supported in part by Sharon L. Cockrell Cancer Research Fund, STOP CANCER Research Career Development Award (to Y. Z.), Department of Defense CDMRP Career Development Award W81XWH-19-1-0272 (to Y.Z.), National Institute of General Medical Sciences (NIGMS) of the National Institutes of Health (NIH) grant R35GM137901 (to Y. Z.), and Tobacco Related-Disease Research Program New Investigator Award T30KT1021 (to Y.Z.).

Author contribution

Z.D., X.N.Z. and Y.Z. designed research; Z.D., X.N.Z., Q.C., F.F., T.H., J.L., A.A., and J.W. performed research; H.P., G.S., J.X., H.J.L., and S.G.L. provided resources and critical insights; Z.D., X.N.Z. and Y.Z. analyzed data; Z.D., X.N.Z. and Y.Z. wrote the manuscript.

Competing interests

The authors declare no competing interests.

References

- (1) Ford, C., Newman, C., Johnson, J., Woodhouse, C., Reeder, T., Rowland, G., and Simmonds, R. (1983) Localisation and toxicity study of a vindesine-anti-CEA conjugate in patients with advanced cancer, *British journal of cancer* 47, 35-42.
- (2) Walter, R. B. (2020) Brief overview of antibody–drug conjugate therapy for acute leukemia, Taylor & Francis.
- (3) Li, F., Sutherland, M. K., Yu, C., Walter, R. B., Westendorf, L., Valliere-Douglass, J., Pan, L., Cronkite, A., Sussman, D., and Klussman, K. (2018) Characterization of SGN-CD123A, a potent CD123-directed antibody–drug conjugate for acute myeloid leukemia, *Molecular cancer therapeutics* 17, 554-564.
- (4) Jain, N., Smith, S. W., Ghone, S., and Tomczuk, B. (2015) Current ADC linker chemistry, *Pharmaceutical research* 32, 3526-3540.
- (5) Hamblett, K. J., Senter, P. D., Chace, D. F., Sun, M. M., Lenox, J., Cerveny, C. G., Kissler, K. M., Bernhardt, S. X., Kopcha, A. K., and Zabinski, R. F. (2004) Effects of drug loading on the antitumor activity of a monoclonal antibody drug conjugate, *Clinical cancer research* 10, 7063-7070.
- (6) Wakankar, A. A., Feeney, M. B., Rivera, J., Chen, Y., Kim, M., Sharma, V. K., and Wang, Y. J. (2010) Physicochemical stability of the antibody– drug conjugate trastuzumab-DM1: changes due to modification and conjugation processes, *Bioconjugate chemistry* 21, 1588-1595.
- (7) Axup, J. Y., Bajjuri, K. M., Ritland, M., Hutchins, B. M., Kim, C. H., Kazane, S. A., Halder, R., Forsyth, J. S., Santidrian, A. F., and Stafin, K. (2012) Synthesis of site-specific antibody-drug conjugates using unnatural amino acids, *Proceedings of the National Academy of Sciences* 109, 16101-16106.

- (8) Bruins, J. J., Westphal, A. H., Albada, B., Wagner, K., Bartels, L., Spits, H., van Berkel, W. J., and van Delft, F. L. (2017) Inducible, site-specific protein labeling by tyrosine oxidation–strain-promoted (4+ 2) cycloaddition, *Bioconjugate chemistry* 28, 1189-1193.
- (9) Li, X., Nelson, C. G., Nair, R. R., Hazlehurst, L., Moroni, T., Martinez-Acedo, P., Nanna, A. R., Hymel, D., Burke Jr, T. R., and Rader, C. (2017) Stable and potent selenomab-drug conjugates, *Cell chemical biology* 24, 433-442. e436.
- (10) Lin, S., Yang, X., Jia, S., Weeks, A. M., Hornsby, M., Lee, P. S., Nichiporuk, R. V., Iavarone, A. T., Wells, J. A., and Toste, F. D. (2017) Redox-based reagents for chemoselective methionine bioconjugation, *Science* 355, 597-602.
- (11) Okeley, N. M., Toki, B. E., Zhang, X., Jeffrey, S. C., Burke, P. J., Alley, S. C., and Senter, P. D. (2013) Metabolic engineering of monoclonal antibody carbohydrates for antibody–drug conjugation, *Bioconjugate chemistry* 24, 1650-1655.
- (12) Tian, F., Lu, Y., Manibusan, A., Sellers, A., Tran, H., Sun, Y., Phuong, T., Barnett, R., Hehli, B., and Song, F. (2014) A general approach to site-specific antibody drug conjugates, *Proceedings of the National Academy of Sciences* 111, 1766-1771.
- (13) VanBrunt, M. P., Shanebeck, K., Caldwell, Z., Johnson, J., Thompson, P., Martin, T., Dong, H., Li, G., Xu, H., and D’Hooge, F. (2015) Genetically encoded azide containing amino acid in mammalian cells enables site-specific antibody–drug conjugates using click cycloaddition chemistry, *Bioconjugate chemistry* 26, 2249-2260.
- (14) Zhou, Q., Stefano, J. E., Manning, C., Kyazike, J., Chen, B., Gianolio, D. A., Park, A., Busch, M., Bird, J., and Zheng, X. (2014) Site-specific antibody–drug conjugation through glycoengineering, *Bioconjugate chemistry* 25, 510-520.
- (15) Zhu, Z., Ramakrishnan, B., Li, J., Wang, Y., Feng, Y., Prabakaran, P., Colantonio, S., Dyba, M. A., Qasba, P. K., and Dimitrov, D. S. (2014) Site-specific antibody-drug conjugation through an engineered glycotransferase and a chemically reactive sugar, In *MAbs*, pp 1190-1200, Taylor & Francis.
- (16) Dennler, P., Chiotellis, A., Fischer, E., Brégeon, D., Belmant, C., Gauthier, L., Lhospice, F., Romagne, F. o., and Schibli, R. (2014) Transglutaminase-based chemo-enzymatic conjugation approach yields homogeneous antibody–drug conjugates, *Bioconjugate chemistry* 25, 569-578.
- (17) Strop, P., Liu, S.-H., Dorywalska, M., Delaria, K., Dushin, R. G., Tran, T.-T., Ho, W.-H., Farias, S., Casas, M. G., and Abdiche, Y. (2013) Location matters: site of conjugation modulates stability and pharmacokinetics of antibody drug conjugates, *Chemistry & biology* 20, 161-167.
- (18) Dorywalska, M., Strop, P., Melton-Witt, J. A., Hasa-Moreno, A., Farias, S. E., Galindo Casas, M., Delaria, K., Lui, V., Poulsen, K., and Sutton, J. (2015) Site-dependent degradation of a non-cleavable auristatin-based linker-payload in rodent plasma and its effect on ADC efficacy, *PLoS One* 10, e0132282.
- (19) Stefan, N., Gébleux, R., Waldmeier, L., Hell, T., Escher, M., Wolter, F. I., Grawunder, U., and Beerli, R. R. (2017) Highly potent, anthracycline-based antibody–drug conjugates generated by enzymatic, site-specific conjugation, *Molecular cancer therapeutics* 16, 879-892.
- (20) Beerli, R. R., Hell, T., Merkel, A. S., and Grawunder, U. (2015) Sortase enzyme-mediated generation of site-specifically conjugated antibody drug conjugates with high in vitro and in vivo potency, *PloS one* 10, e0131177.
- (21) Woitok, M., Klose, D., Di Fiore, S., Richter, W., Stein, C., Gresch, G., Grieger, E., Barth, S., Fischer, R., and Kolberg, K. (2017) Comparison of a mouse and a novel human scFv-SNAP-auristatin F drug conjugate with potent activity against EGFR-overexpressing human solid tumor cells, *Oncotargets and therapy* 10, 3313.

- (22) Nanna, A. R., Li, X., Walseng, E., Pedzisa, L., Goydel, R. S., Hymel, D., Burke Jr, T. R., Roush, W. R., and Rader, C. (2017) Harnessing a catalytic lysine residue for the one-step preparation of homogeneous antibody-drug conjugates, *Nature communications* 8, 1112.
- (23) Dai, Z., Zhang, X.-N., Nasertorabi, F., Cheng, Q., Li, J., Katz, B. B., Smbatyan, G., Pei, H., Louie, S. G., and Lenz, H.-J. (2020) Synthesis of site-specific antibody-drug conjugates by ADP-ribosyl cyclases, *Science Advances* 6, eaba6752.
- (24) Lowenberg, B., Downing, J. R., and Burnett, A. (1999) Acute myeloid leukemia, *New England Journal of Medicine* 341, 1051-1062.
- (25) Bakker, A. B., van den Oudenrijn, S., Bakker, A. Q., Feller, N., van Meijer, M., Bia, J. A., Jongeneelen, M. A., Visser, T. J., Bijl, N., and Geuijen, C. A. (2004) C-type lectin-like molecule-1: a novel myeloid cell surface marker associated with acute myeloid leukemia, *Cancer research* 64, 8443-8450.
- (26) Lin, T.-y., Zhu, Y., Li, Y., Zhang, H., Ma, A.-H., Long, Q., Keck, J., Lam, K. S., Pan, C.-x., and Jonas, B. A. (2019) Daunorubicin-containing CLL1-targeting nanomicelles have anti-leukemia stem cell activity in acute myeloid leukemia, *Nanomedicine: Nanotechnology, Biology and Medicine* 20, 102004.
- (27) Lu, H., Zhou, Q., Deshmukh, V., Phull, H., Ma, J., Tardif, V., Naik, R. R., Bouvard, C., Zhang, Y., and Choi, S. (2014) Targeting human C-type lectin-like molecule-1 (CLL1) with a bispecific antibody for immunotherapy of acute myeloid leukemia, *Angewandte Chemie International Edition* 53, 9841-9845.
- (28) De Togni, E., Kim, M. Y., Cooper, M. L., Ritchey, J., O'Neal, J., Niswonger, J., and DiPersio, J. F. (2018) Chimeric Antigen Receptor T Cells Specific for CLL-1 for Treatment of Acute Myeloid Leukemia, *Blood* 132, 2205-2205.
- (29) Jiang, Y.-P., Liu, B. Y., Zheng, Q., Panuganti, S., Chen, R., Zhu, J., Mishra, M., Huang, J., Dao-Pick, T., and Roy, S. (2018) CLT030, a leukemic stem cell-targeting CLL1 antibody-drug conjugate for treatment of acute myeloid leukemia, *Blood advances* 2, 1738-1749.
- (30) Zheng, B., Yu, S.-F., Del Rosario, G., Leong, S. R., Lee, G. Y., Vij, R., Chiu, C., Liang, W.-C., Wu, Y., and Chalouni, C. (2019) An Anti-CLL-1 Antibody-Drug Conjugate for the Treatment of Acute Myeloid Leukemia, *Clinical Cancer Research* 25, 1358-1368.
- (31) Zhao, X., Singh, S., Pardoux, C., Zhao, J., Hsi, E. D., Abo, A., and Korver, W. (2010) Targeting C-type lectin-like molecule-1 for antibody-mediated immunotherapy in acute myeloid leukemia, *Haematologica* 95, 71-78.

Supporting Information

Site-Specific Antibody-Drug Conjugates with Variable Drug-to-Antibody-Ratios for Acute Myeloid Leukemia Therapy

Zhefu Dai^{1#}, Xiao-Nan Zhang^{1#}, Qinqin Cheng¹, Fan Fei¹, Tianling Hou¹, Jiawei Li¹, Alireza Abdolvahabi², Junji Watanabe³, Hua Pei⁴, Goar Smbatyan⁵, Jianming Xie¹, Heinz-Josef Lenz⁵, Stan G. Louie⁴ and Yong Zhang^{1,6,7,8*}

¹Department of Pharmacology and Pharmaceutical Sciences, School of Pharmacy, University of Southern California, Los Angeles, CA 90089, USA

²Mass Spectrometry Core Facility, School of Pharmacy, University of Southern California, Los Angeles, CA 90089, USA

³Translational Research Laboratory, School of Pharmacy, University of Southern California, Los Angeles, CA 90089, USA

⁴Titus Family Department of Clinical Pharmacy, School of Pharmacy, University of Southern California, Los Angeles, CA 90089, USA

⁵Division of Medical Oncology, Norris Comprehensive Cancer Center, Keck School of Medicine, University of Southern California, Los Angeles, CA 90089, USA

⁶Department of Chemistry, Dornsife College of Letters, Arts and Sciences, University of Southern California, Los Angeles, CA 90089, USA

⁷Norris Comprehensive Cancer Center, University of Southern California, Los Angeles, CA 90089, USA

⁸Research Center for Liver Diseases, University of Southern California, Los Angeles, CA 90089, USA

[#]These authors contributed equally to this work

*Corresponding author. Email: yongz@usc.edu

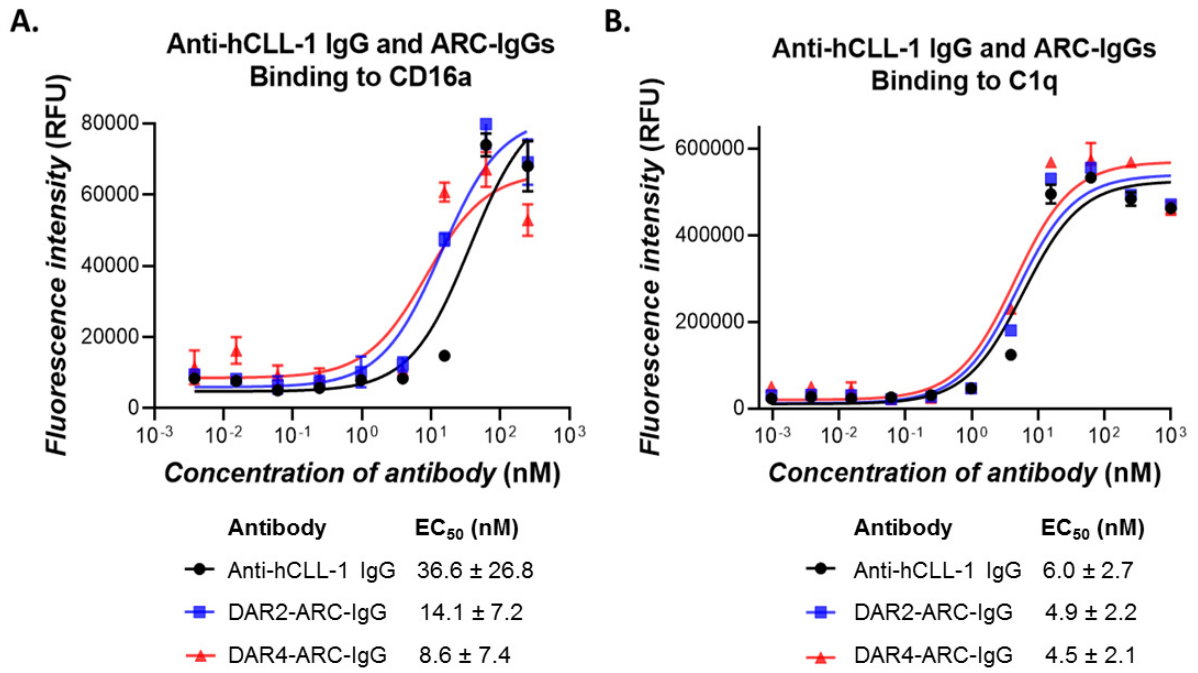


Figure S1. ELISA analysis of binding to human CD16a (A) and C1q protein (B).

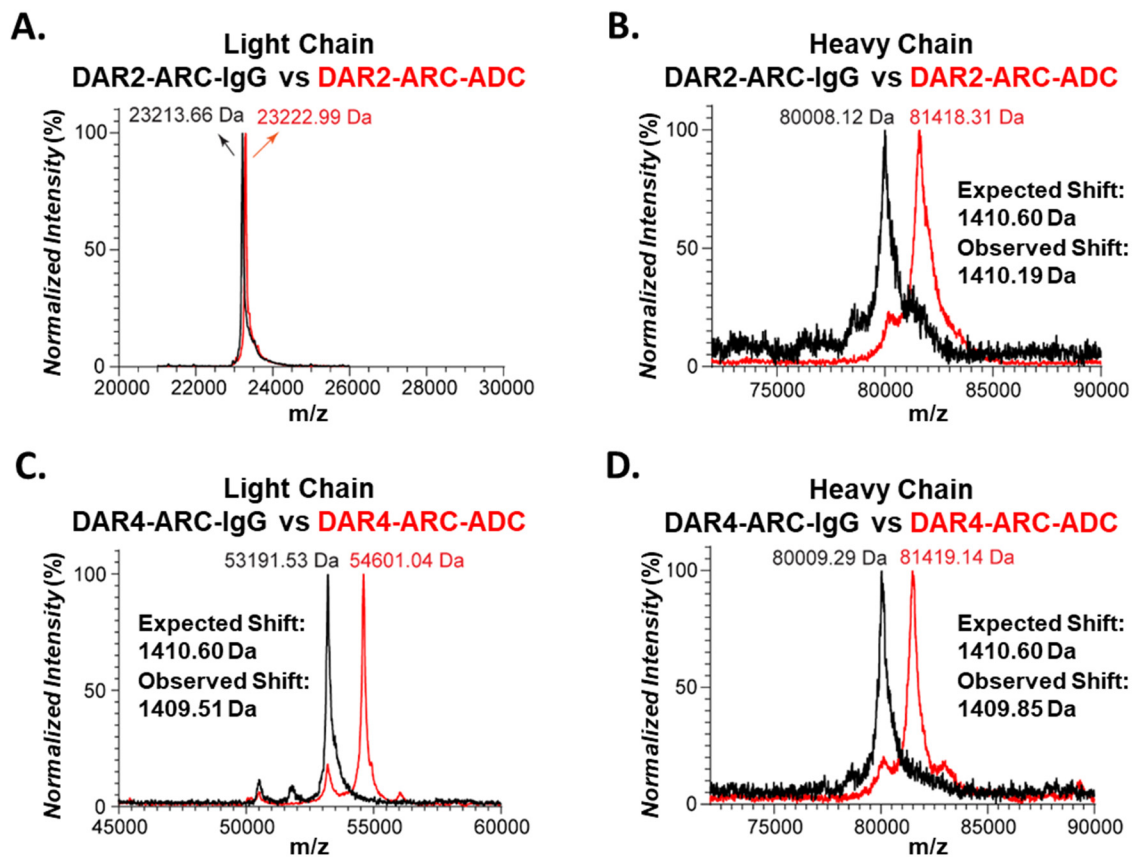


Figure S2. MALDI-TOF mass spectra of light chain and heavy chain of DAR2-ARC-IgG, DAR2-ARC-ADC, DAR4-ARC-IgG, and DAR4-ARC-ADC.

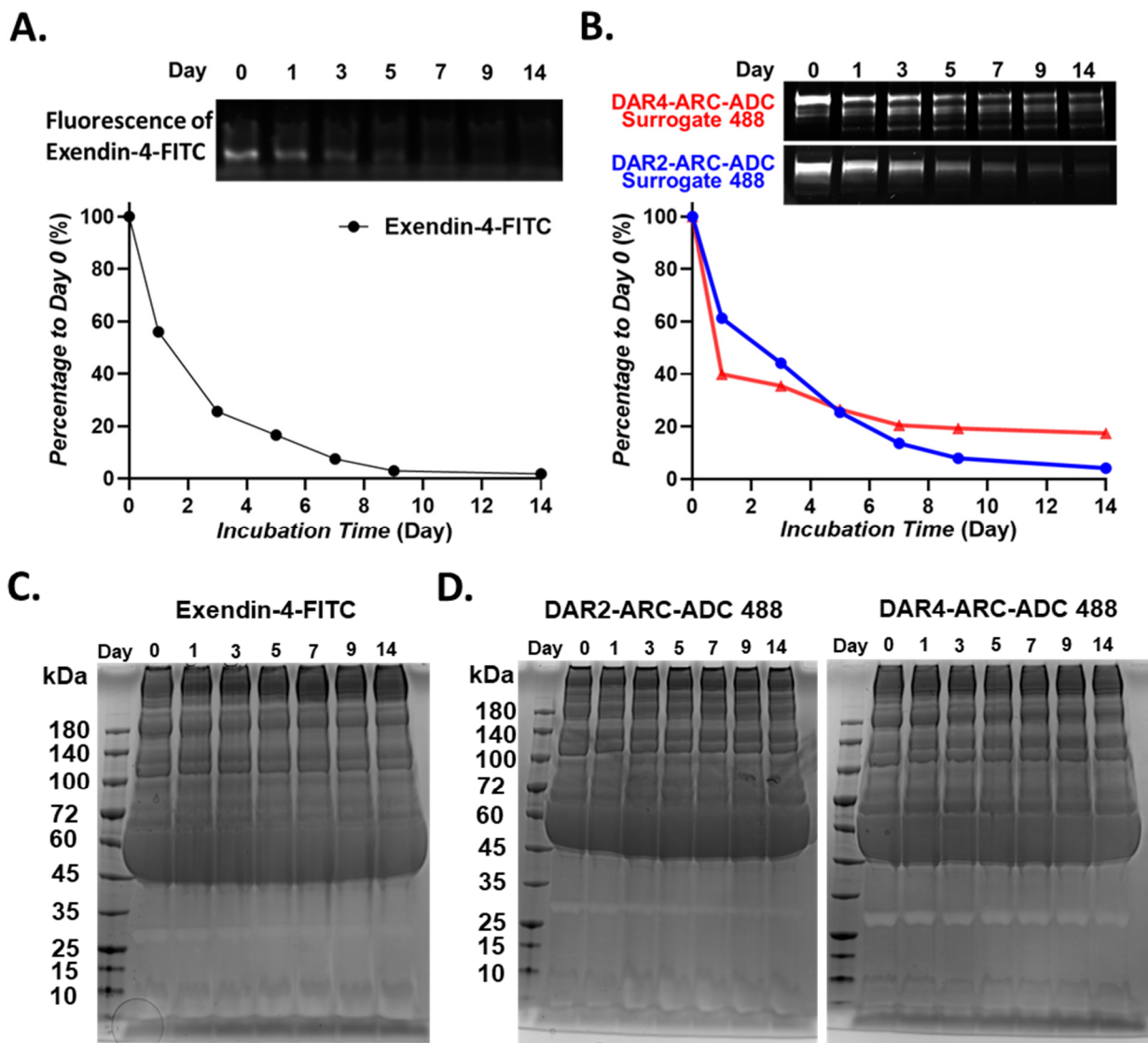


Figure S3. Stability in mouse plasma for surrogate DAR2-ARC-ADC and DAR4-ARC-ADC with Alexa Fluor 488 as the payloads. (A) Stability of fluorescein-labeled exendin-4 in mouse plasma. Upper panel: in-gel fluorescence imaging; lower panel: quantification of fluorescence intensities for intact fluorescein-labeled exendin-4 in mouse plasma. (B) Stability of surrogate DAR2-ARC-ADC and DAR4-ARC-ADC with Alexa Fluor 488. Upper panel: in-gel fluorescence imaging; lower panel: quantification of fluorescence intensities for intact surrogate ARC-ADCs in mouse plasma. (C) A Coomassie blue-stained SDS-PAGE gel for fluorescein-labeled exendin-4 in mouse plasma. (D) Coomassie blue-stained SDS-PAGE gels for surrogate ARC-ADCs.

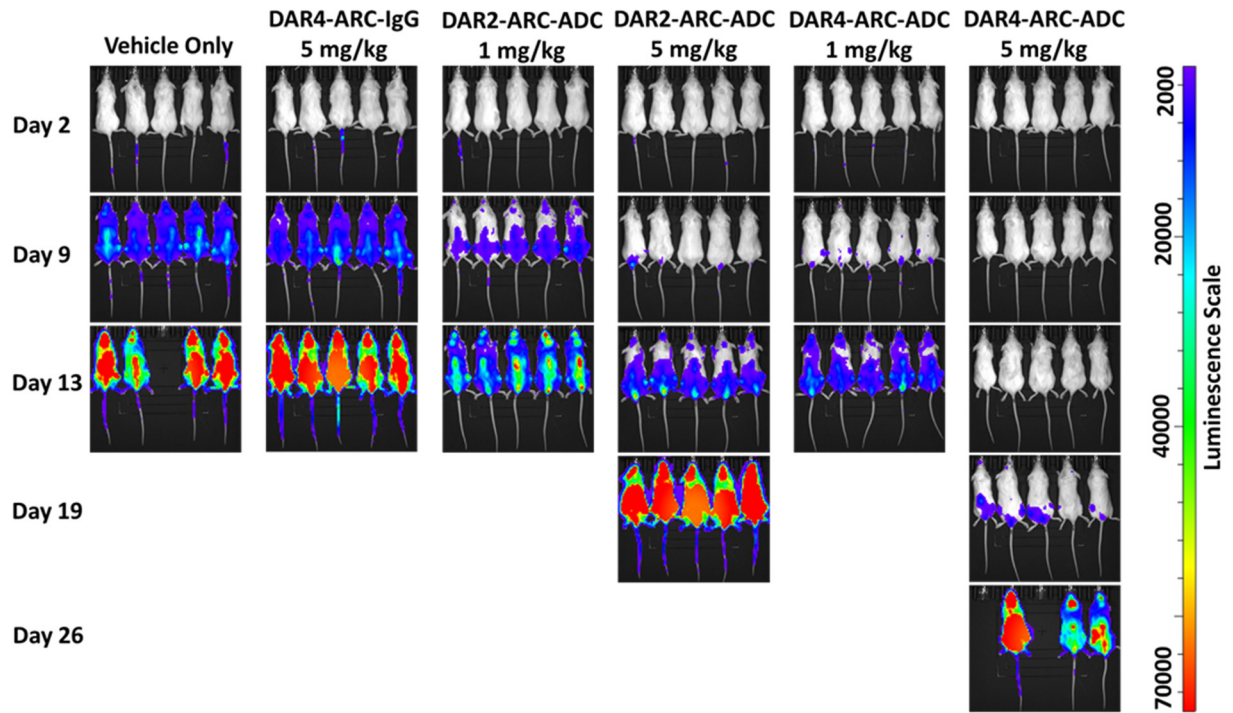


Figure S4. IVIS images for mice from all treatment groups of the *in vivo* efficacy study. IVIS imaging was started on day 2 post i.v. inoculation of luciferase-expressing U937 cells and continued on a weekly basis.

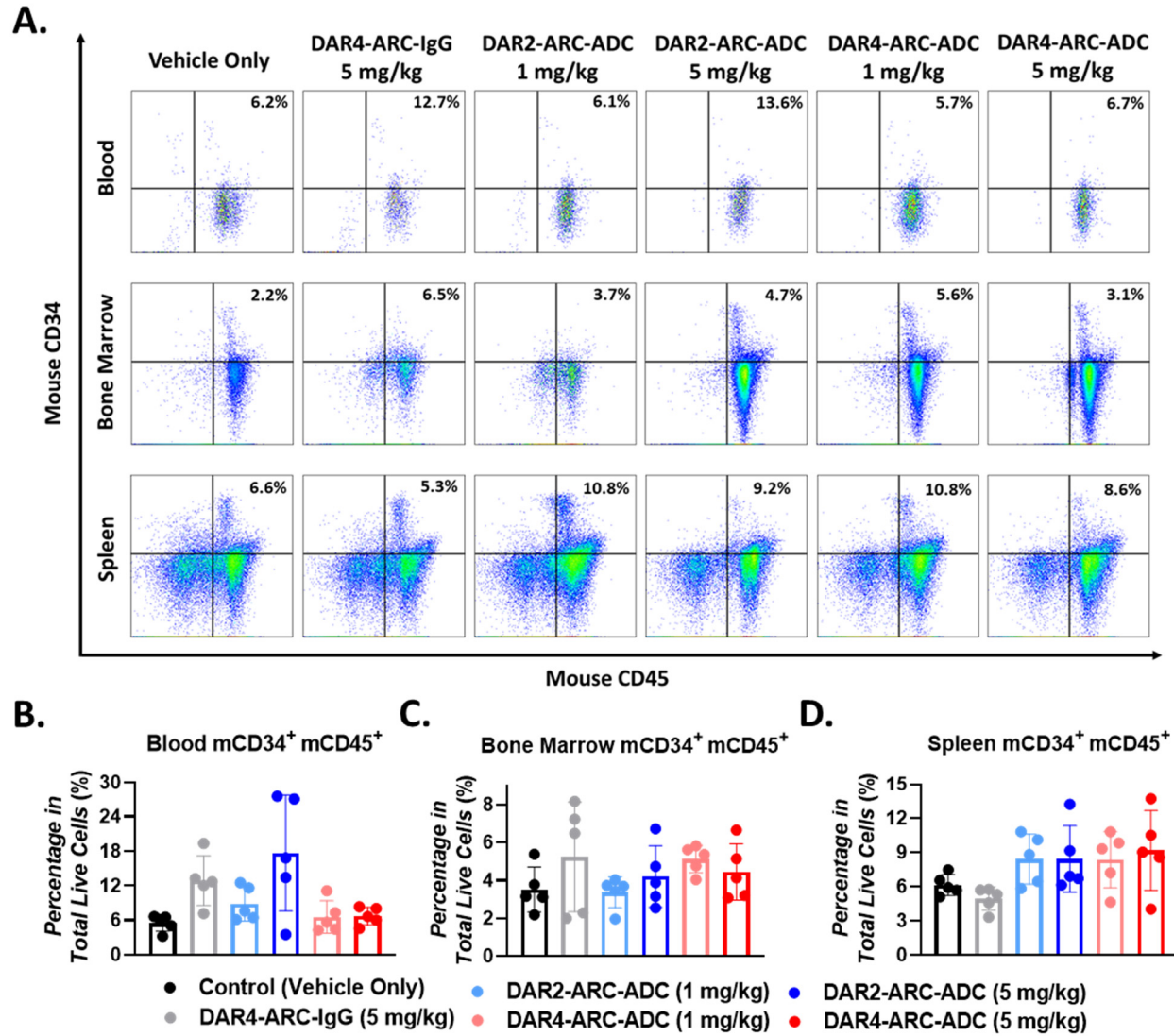
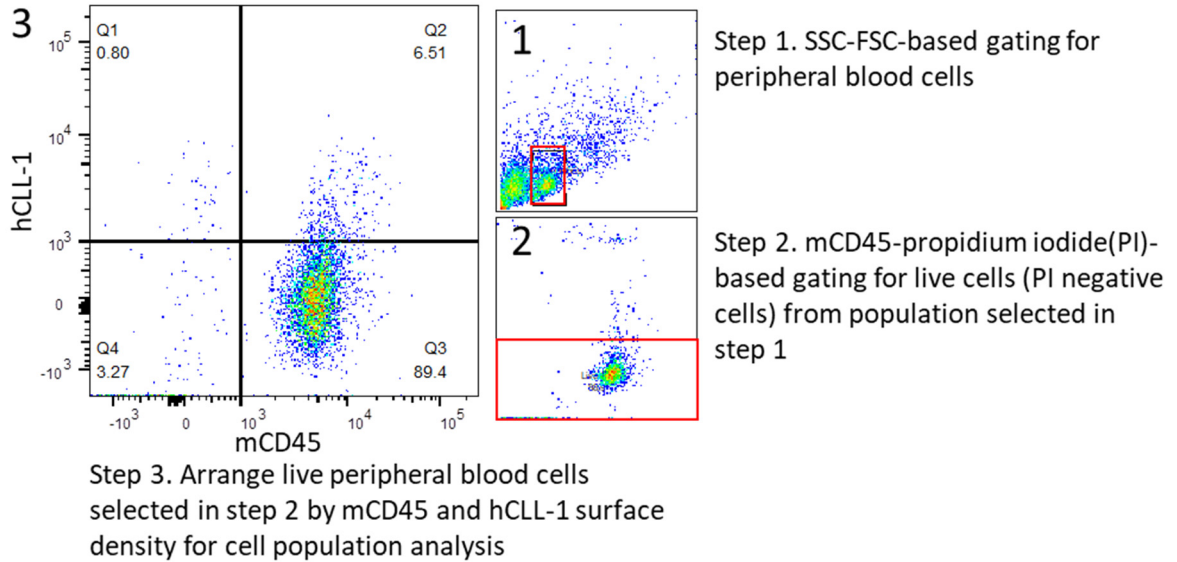


Figure S5. Flow cytometric analysis of tissue samples collected on day 13 post U937 implantation. (A) Representative flow cytometry data for percentages of mCD34⁺ mCD45⁺ cell population in total living cells in blood, bone marrow, and spleen among different treatment groups. (B-D) Percentages of mCD34⁺ mCD45⁺ cells in total living cells in blood (B), bone marrow (C), and spleen (D) among different treatment groups.

Gating of Blood Samples by mCD45 and hCLL-1



Gating of Blood Samples by mCD45 and mCD34

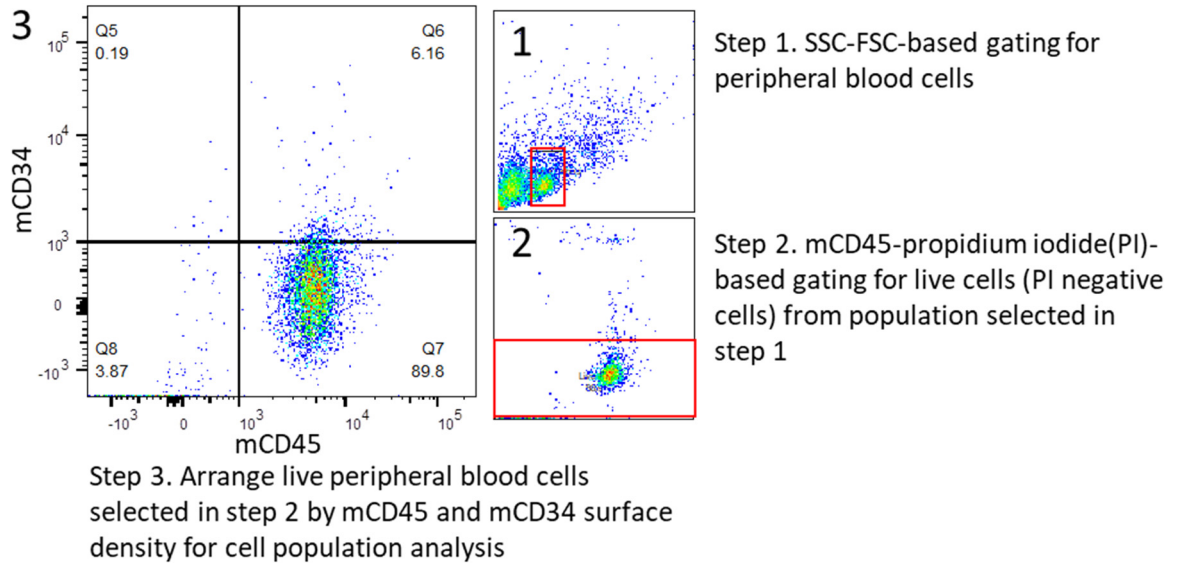
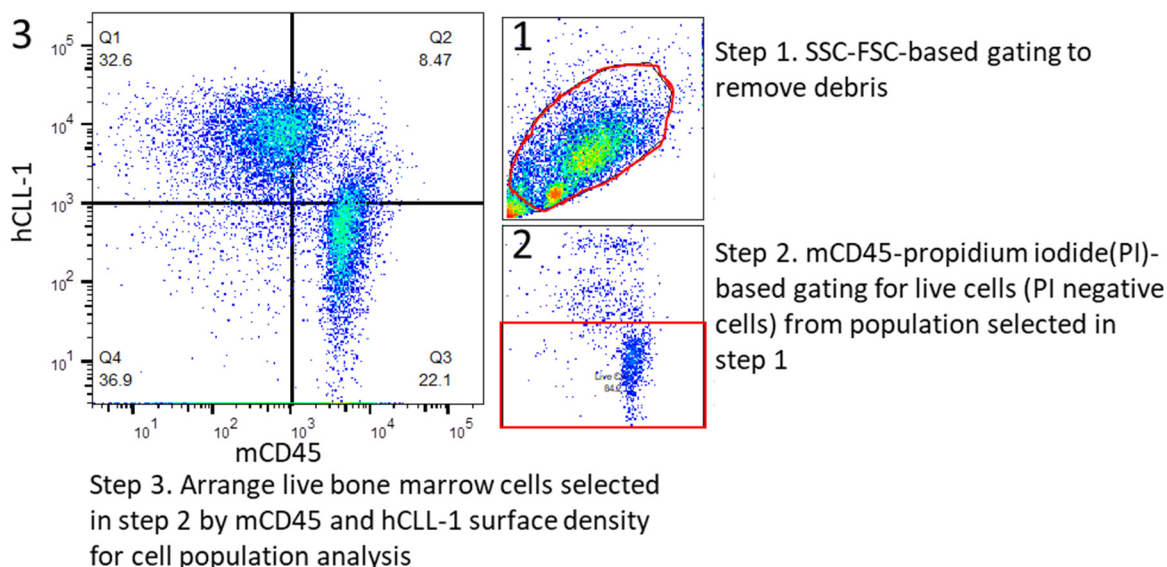


Figure S6. Gating strategies for blood samples analyzed by flow cytometry.

Gating of Bone Marrow Samples by mCD45 and hCLL-1



Gating of Bone Marrow Samples by mCD45 and mCD34

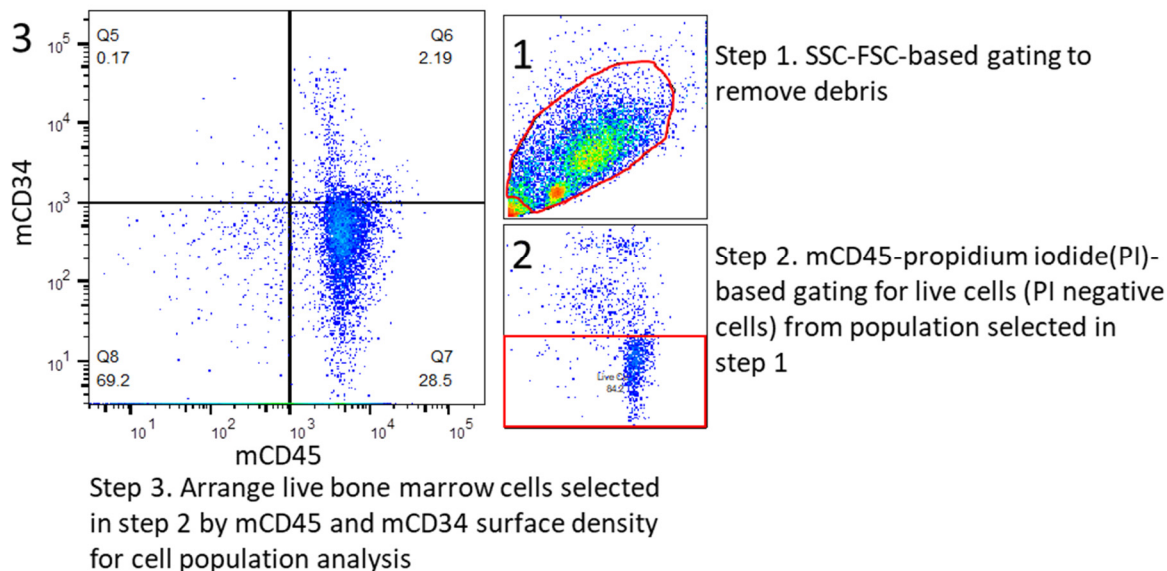
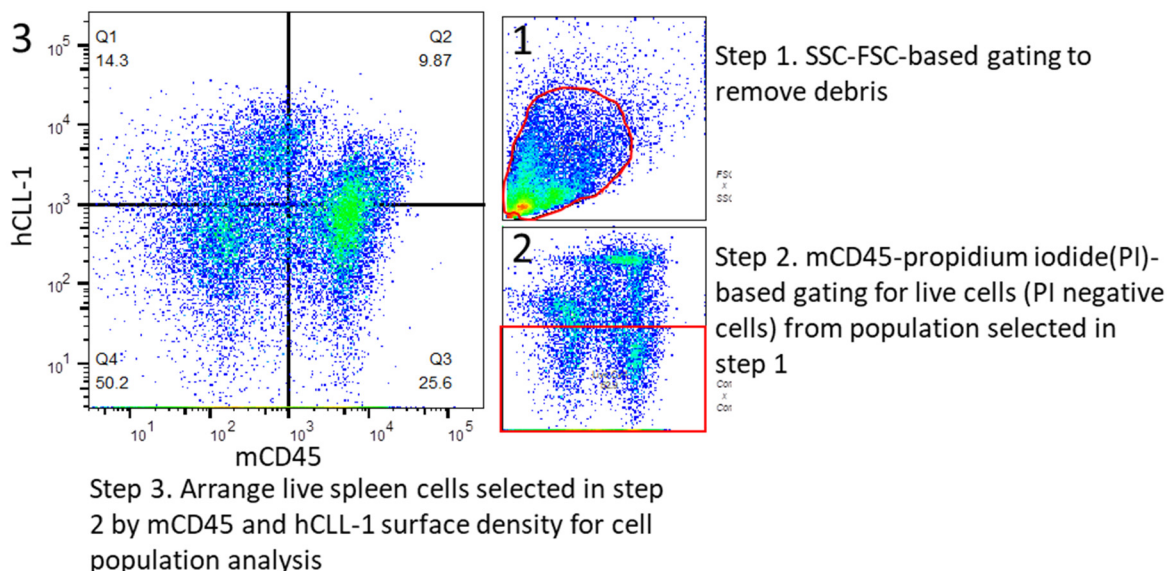


Figure S7. Gating strategies for bone marrow samples analyzed by flow cytometry.

Gating of Spleen Samples by mCD45 and hCLL-1



Gating of Spleen Samples by mCD45 and mCD34

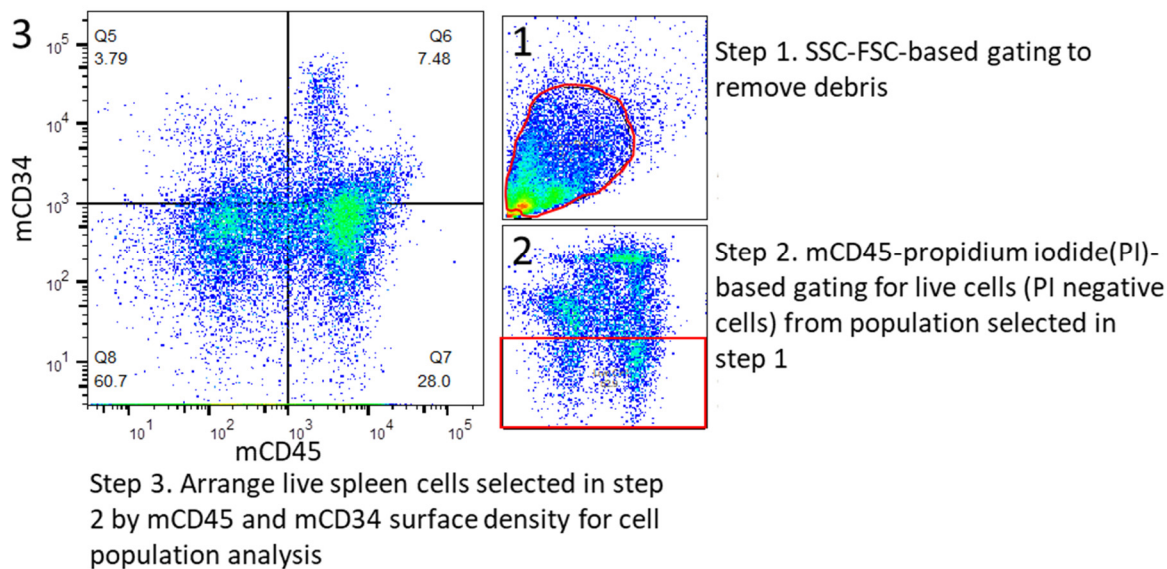


Figure S8. Gating strategies for spleen samples analyzed by flow cytometry.